Journal Publication of International Research for Engineering and Management (JOIREM)
Volume: 04 Issue: 03 | Mar-2026
ISSN (O) 3107-6696

Investigating Direct Current Stimulation of Wounded Cell Collectives via Bioelectronic Microfluidic Wound Healing: A Review

Prannesh U R[1], Siya Saji[2], Reshma Banu S[3], Akshay Krishanan U S[4], Ramachandhran A M[5]

[1,2,3,4]*Post Graduate Student, Department of Microbiology, Dr. N.G.P. Arts and Science College*
[5]*Associate Professor, Department of Microbiology, Dr. N.G.P. Arts and Science College*
prannesh12345@gmail.com

Abstract - Upon cutaneous injury, the human body naturally heals the injured area by developing an endogenous electric field (EF) that guides cellular and tissue repair complexes towards the wound site. The resulting Direct Current (DC) ionic flow, generated by disruption of the transepithelial potential, influences a variety of biological processes relevant to wound repair. This DC stimulation can impact both diabetic and healthy in vitro keratinocyte tissues to clarify the effects of EF/DC stimulation on wound healing dynamics. Keratinocytes constitute the predominant cell type in the human epidermis, forming densely packed lateral layers that migrate collectively during wound closure. A bioelectronic microfluidic platform was developed to study the effects of different EF spatial configurations on wound gap closure using non-metal, pseudocapacitive PEDOT:PSS hydrogel-coated laser-induced graphene electrodes combined with prudent microfluidic channel architecture. Two spatial stimulation strategies were rigorously examined: unidirectional EF (electrotactically closing a wound from one edge) versus pseudo- converging EF (alternately polarizing both wound edges). Unidirectional electrical guidance cues proved superior in driving collective keratinocyte healing dynamics, accelerating wound closure rates by approximately three-fold for both healthy and diabetic-like keratinocyte collectives compared to pseudo- converging EF and non-stimulated controls. Under unidirectional electrical stimulation, motility- inhibited diabetic-like keratinocytes recovered wound closure rates (increasing from 1.0 to 2.8% h^{-1}) comparable to healthy, non-stimulated counterparts (3.5% h^{-1}). The results support the hypothesis that regulated electrical stimulation represents a practical therapeutic strategy for accelerating wound healing, particularly in chronic wound contexts. These findings also establish a translational baseline for optimizing electrode design for in vivo DC stimulation applications in regenerative medicine.

Keywords: *wound healing; electric field stimulation; electrotaxis; microfluidics; keratinocytes; PEDOT:PSS; laser-induced graphene; bioelectronics; diabetic wound model; collective cell migration*

1. Introduction

For the majority of individuals, a wound is typically a minor issue that heals naturally without requiring extensive medical intervention. However, for people with chronic illnesses such as diabetes mellitus and peripheral vascular disease, individuals with weakened immune systems such as systemic lupus erythematosus, or those experiencing systemic challenges including malnutrition and aging, the healing process of acute wounds is significantly hindered.[1,2] This substantially increases the likelihood of acute wounds transitioning into chronic, non-healing wounds—a major clinical challenge worldwide.

The high prevalence of chronic wounds presents a significant socioeconomic challenge, contributing to approximately 1 to 3% of overall healthcare costs in developed countries.[1] This financial burden continues to grow in parallel with the rising median age of global populations. The number of individuals suffering from diabetic foot ulcers alone is estimated to exceed 400 million worldwide, with the condition representing the leading cause of non-traumatic lower-limb amputation.[3] In addition to the economic impact, chronic wounds impose considerable patient distress, significantly reducing quality of life. Therefore, the development of innovative strategies to enhance wound healing, particularly in vulnerable populations, has emerged as an urgent clinical and research priority. Wound healing is a complex, highly coordinated biological process typically divided into four sequential yet overlapping stages: hemostasis, inflammation, proliferation, and maturation.[4] Each stage involves distinct cellular participants engaging in a coordinated manner to facilitate tissue repair, including activated platelets, neutrophils, monocytes, macrophages, mast cells, dendritic cells, T cells, endothelial cells, fibroblasts, myofibroblasts, and keratinocytes.[4,5] Throughout the healing process, these cells are recruited from adjacent tissues or distant locations via the circulatory system, guided by a

constellation of biochemical, mechanical, and electrical signals.

Cell migration toward the wound site is regulated by processes including chemotaxis (chemical gradient-mediated), haptotaxis or durotaxis (extracellular matrix and substrate stiffness-mediated), and electrotaxis or galvanotaxis (electric field-mediated).[6,7] Several critical cell types involved in wound healing— neutrophils, monocytes, lymphocytes, macrophages, endothelial cells, fibroblasts, and keratinocytes— exhibit electrotactic behavior.[8,9] Importantly, wounds naturally generate small endogenous electric fields following disruption of the epithelial layer, and these fields are now recognized as important biological cues directing the wound healing response.[10,15] Under normal physiological conditions, the skin maintains a transepithelial potential difference ranging between approximately 10 mV and 60 mV due to active inward transport of sodium ions (Na^+) and outward transport of chloride ions (Cl^-). When a wound occurs, this potential difference is disrupted, generating a positive ionic current that flows radially toward the wound center.[15,16] The strength of these endogenous EFs varies significantly between individuals; lateral electric fields in younger individuals aged 18–25 years (107–148 mV mm^{-1}) are approximately 48% stronger than those in older individuals aged 65–80 years (56–76 mV mm^{-1}).[16] This age-related reduction in endogenous EF strength may partly explain the well-documented impairment of wound healing in elderly patients.

The application of exogenous direct current (DC) electric fields to wounds has gained considerable interest as a supplementary therapeutic modality. Research suggests that applied ionic flow, regardless of EF directionality, serves as a key driver in accelerating wound closure through activation of mitogen- activated protein kinase (MAPK) signaling pathways and rapid reorganization of cellular structures.[19,20] Keratinocytes, the predominant cell type in the skin (~90% of the epidermis), exhibit collective migration behavior within densely packed lateral layers—a biologically relevant model that differs substantially from single-cell migration studies.[22]

The present review critically examines the bioelectronic microfluidic platform developed to investigate the effects of precisely controlled DC electric field stimulation on wound closure dynamics in both healthy and diabetic-like keratinocyte collectives. We discuss the design rationale for the 'peace sign' microfluidic architecture, the development and characterization of PEDOT:PSS hydrogel-coated laser-induced graphene (LIG) electrodes, and the comparative effectiveness of unidirectional versus pseudo- converging EF configurations. Additionally, we contextualize these findings within the broader landscape of bioelectricity in wound healing, drawing on published literature to identify key mechanistic insights and future translational opportunities. The primary objectives of this work are: (a) to examine the role of electrical guidance cues, particularly EF spatial distribution, in determining wound closure rate; (b) to develop a stable, biocompatible non-metal DC stimulation electrode without salt bridges; and (c) to establish a diabetic keratinocyte wound model to assess whether EF stimulation can enhance healing under conditions of impaired motility.

2. Background: Bioelectricity and Wound Healing

2.1 Historical Perspective on Electrical Stimulation in Medicine

The therapeutic application of electricity to living tissues has a long and evolving history. Early observations by Galvani (1791) and Volta (1800) laid the conceptual groundwork for bioelectricity.[17] Clinical interest in electrical stimulation for wound healing surged in the mid-twentieth century, driven by empirical observations that bone fractures and soft-tissue wounds healed more rapidly when exposed to exogenous electrical currents. Landmark studies by Fukada and Yasuda (1957) on piezoelectricity in bone, followed by Becker and Murray's demonstration of bioelectric potentials in regenerating tissues, established a scientific basis for bioelectric medicine.[17] By the 1970s and 1980s, clinical reports documented accelerated wound healing in chronic pressure ulcers, venous leg ulcers, and diabetic foot ulcers treated with various forms of electrical stimulation, including high-voltage pulsed current (HVPC), low-intensity direct current (LIDC), and transcutaneous electrical nerve stimulation (TENS).[21]

Despite this historical evidence base, widespread clinical adoption of electrostimulation for wound healing has been hampered by a lack of standardization in stimulation parameters, inconsistent results across trials, and an incomplete mechanistic understanding of how electrical fields interact with wound biology at the cellular and molecular levels.[21] The emergence of precision microfluidic platforms and conducting polymer electrode materials in the past decade has created new opportunities to revisit and systematically interrogate bioelectric wound

healing mechanisms with unprecedented experimental control.

2.2 Endogenous Electric Fields in Skin: The Wound Current

The skin is an electrically active tissue. Epithelial cells actively transport ions across their membranes, creating a transepithelial potential (TEP) that is negative on the inner (basal) side relative to the outer surface. In mammalian skin, this TEP ranges from approximately −15 mV to −70 mV (inside negative), maintained primarily by the apical Na^+/K^+-ATPase and basolateral Cl^- channels.[15] The high electrical resistance of the intact stratum corneum prevents current leakage, preserving this potential difference across the full thickness of the epidermis.

When the skin is wounded, the high-resistance epithelial barrier is broken, creating a low-resistance pathway for ionic current flow. Positive current (carried principally by Na^+ and K^+ ions) flows outward from the wound center, while electrons (in current terms) flow inward. This produces a lateral electric field in the tissue flanking the wound, with the wound center acting as a current sink (cathode) and the surrounding intact tissue acting as a source (anode).[15,35] Measured lateral EF strengths at wound edges in human skin range from approximately 40 to 200 mV mm^{-1}, depending on location, tissue type, and individual biological variability.[16]

Several lines of evidence confirm the biological significance of the wound current: (i) pharmacological disruption of epithelial ion transport reduces both the wound EF and the rate of healing; (ii) enhancing ion transport pharmacologically increases EF strength and accelerates closure; and (iii) genetic ablation of key ion channels impairs electrotaxis in wound-healing cell lines.[15,19,20] These findings collectively establish the endogenous wound current as a critical directional cue orchestrating the cellular migration that underlies wound repair.

2.3 Types of Exogenous Electrical Stimulation

Various modalities of exogenous electrical stimulation have been investigated for wound healing applications, each with distinct parameters, mechanisms, and clinical evidence bases:

Direct Current (DC) Stimulation: Continuous unidirectional ionic flow. Low-intensity DC (~0.1–1.0 mA) has been shown to accelerate wound healing by enhancing electrotaxis, activating MAPK pathways, and promoting angiogenesis.[19,21] However, prolonged DC stimulation risks faradaic electrode reactions that alter local pH and introduce toxic by-products—a key challenge addressed in the present study.

High-Voltage Pulsed Current (HVPC): Monophasic pulsed DC with peak voltages of 100–500 V and pulse durations of 40–200 µs. HVPC has demonstrated efficacy in clinical trials for pressure ulcers and venous leg ulcers, reducing healing time and wound area.[21] Its high peak voltage promotes bactericidal effects and antimicrobial action in addition to electrotactic cell guidance.

Alternating Current (AC) and Pulsed Electromagnetic Field (PEMF): Sinusoidal or pulsed bidirectional currents that avoid electrochemical by-products. PEMF has been employed in orthopedic applications and is under investigation for soft-tissue wound healing, particularly for its anti-inflammatory effects.[21]

Transcutaneous Electrical Stimulation (TES): Non-invasive surface electrodes delivering current through intact or minimally disrupted skin. TES has shown benefit in pressure ulcers in paraplegic patients and in diabetic foot wound care protocols.[66]

3. Cellular and Molecular Mechanisms of Electrotaxis

3.1 Single-Cell Electrotaxis vs. Collective Migration

Electrotaxis—the directed migration of cells in response to an applied EF—has been documented in numerous cell types relevant to wound healing.[8] Early in vitro studies primarily examined single-cell electrotaxis using keratinocytes, fibroblasts, endothelial cells, and immune cells individually. These studies established fundamental parameters such as threshold EF strengths (~10–50 mV mm^{-1}), optimal EF magnitudes (100–300 mV mm^{-1}), and cell-type-specific directionality (cathodic for keratinocytes and endothelial cells; anodic for certain fibroblast subtypes).[42,43]

However, single-cell models fail to capture the coordinated behavior of keratinocytes within intact epithelium. In confluent monolayers, keratinocyte migration is governed by collective dynamics: leader cells at the wound periphery extend lamellipodia and generate traction forces transmitted via cell–substrate adhesions (focal adhesions) and cell–cell junctions (adherens junctions mediated by E- cadherin).[25,26] Follower cells are mechanically coupled to leaders, propagating forces across the sheet in a coordinated wave-like manner. This

collective mode of migration more accurately represents the re-epithelialization process observed in vivo, where the advancing epithelial front moves as a continuous sheet rather than as isolated cells.[26]

The first documented observation of collective keratinocyte electrotaxis was reported by Zhao et al.[27], who demonstrated cathodic collective migration in keratinocyte monolayers exposed to 100–300 mV mm^{-1} EFs. Subsequent work by Zajdel et al.[41] showed that two keratinocyte monolayers separated by a 1.5 mm wound gap closed the wound at twice the rate of unstimulated controls when exposed to 200 mV mm^{-1} DC EF. These foundational studies established collective keratinocyte electrotaxis as a biologically relevant and clinically promising phenomenon.

3.2 Intracellular Signaling Pathways

The cellular response to applied EFs involves a complex network of intracellular signaling cascades. The leading mechanistic hypotheses implicate asymmetric redistribution of membrane receptors and their downstream effectors as primary drivers of electrotactic directionality:

EGFR/PI3K/PTEN axis: EF exposure causes asymmetric accumulation of epidermal growth factor receptor (EGFR) and phosphatidylinositol-3-kinase (PI3K) at the cathodal-facing membrane, while the phosphatase PTEN is enriched at the anodal-facing side. This asymmetry generates a PIP3 gradient that polarizes downstream effectors including Rac1, Cdc42, and Rho GTPases, driving lamellipodial protrusion toward the cathode.[56,57]

MAPK/ERK pathway: Applied ionic flow, independent of EF directionality, activates mitogen-activated protein kinase (MAPK)/extracellular signal-regulated kinase (ERK) signaling, promoting cell cycle entry, proliferation, and cytoskeletal reorganization. This pathway appears to be a primary driver of enhanced wound closure observed under exogenous DC stimulation.[19,20] Critically, the p38 MAPK sub-pathway governs the transition of keratinocytes from a terminally differentiated phenotype to a migratory wound- healing phenotype—a transition that is suppressed in diabetic conditions.[49,50]

AMPK pathway and CD9 regulation: Recent work has demonstrated that DC EF exposure (200 mV mm^{-1}) downregulates CD9 expression—a gene encoding a tetraspanin protein that suppresses keratinocyte migration when upregulated—through activation of the 5'-adenosine monophosphate-activated protein kinase (AMPK) pathway.[55] Since p38/MAPK inhibition increases CD9 expression, EF-mediated AMPK activation provides an alternative route to override migration inhibition, offering a mechanistic basis for EF-based rescue of impaired keratinocyte motility in diabetic conditions.

Calcium signaling: EF stimulation and mechanical wounding both trigger intracellular calcium (Ca^{2+}) waves that propagate through keratinocyte monolayers via gap junctions. Elevated Ca^{2+} enhances cadherin-mediated cell-cell adhesion, modulates focal adhesion dynamics, and regulates cytoskeletal contractility. Interestingly, Shim et al.[58] demonstrated that increased calcium levels reduce individual keratinocyte migration speed and diminish directional response to EF, highlighting a complex interplay between cell-cell cohesion and electrotactic guidance.

3.3 The Role of Kenotaxis and Mechanical Signals

Beyond electrotaxis, keratinocyte migration at wound edges is governed by complementary physical cues. Kenotaxis—the tendency of cells to migrate into free space—generates a 'tissue pressure wave' that propagates from the wound edge inward through the monolayer.[24] This mechanical signal is transmitted via cell–cell stress at adherens junctions and via cell–substrate traction forces mediated by integrins. Leader cells at the wound front exhibit higher traction forces and more persistent migration than follower cells; this heterogeneity in mechanical force generation drives coordinated collective movement.[26]

The interplay between electrical guidance cues and mechanical signals is not fully understood. However, the present study's observation that unidirectional EF outperforms pseudo-converging EF in accelerating wound closure suggests that steady, directional ionic flow engages both electrotactic polarization and kenotactic mechanical signaling in a synergistic manner, while the transient polarity reversals in alternating stimulation may disrupt the mechanical coherence of the advancing epithelial sheet.

4. Electric Field Parameters Governing Wound Closure

4.1 Field Strength and Dose-Response Relationships

The relationship between applied EF strength and electrotactic response is non-linear and cell-type dependent. For human keratinocytes, the threshold EF for detectable electrotaxis is approximately 10–25 mV mm^{-1}, with maximal directional response typically observed between 100 and 300 mV mm^{-1}.[41,42,43] Above approximately 400–600 mV mm^{-1}, cytotoxicity and non-specific membrane effects begin to confound electrotactic measurements. An EF of 200 mV mm^{-1} at the wound center—the value targeted in this study—represents a well-validated, physiologically relevant target within the optimal stimulation range.

In collective keratinocyte monolayers, the EF dose-response relationship has a distinct character compared to single cells. Zajdel et al.[41] reported that monolayer wound closure rate scales approximately linearly with EF strength between 50 and 200 mV mm^{-1}, with diminishing returns at higher field strengths. The present study's wound closure rate of ~10.5% h^{-1} under unidirectional 200 mV mm^{-1} stimulation is consistent with this dose-response relationship and represents a clinically meaningful ~3- fold improvement over the unstimulated rate of ~3.5% h^{-1}.

4.2 EF Directionality: Unidirectional vs. Converging Fields

The spatial distribution of the applied EF determines which wound edges receive directional migration cues and in what direction. In a unidirectional EF configuration—where a single cathode is placed on one side of the wound—the EF vectors are parallel to the wound axis, directing cathodic keratinocyte migration from the anode-side wound edge toward the cathode, while the cathode-side wound edge migrates against the EF. In a converging EF—where the wound center acts as a net cathode—EF vectors point inward from both wound edges, theoretically directing both edges toward the center simultaneously.[31]

Based on single-cell electrotaxis principles, converging EFs would be predicted to produce faster wound closure than unidirectional EFs, as both wound edges receive pro-migratory cathodic cues. However, experimental results in the present study—and in prior work by Zajdel et al.[41]—consistently demonstrate that unidirectional EF produces superior wound closure. This counterintuitive result points to the importance of collective migration dynamics: the mechanical coherence of the epithelial sheet, the polarization of leader cells, and the propagation of force through cell-cell junctions all depend on sustained, unidirectional guidance signals. Periodic reversal of the dominant migration direction in pseudo-converging EF disrupts leader cell polarization and may generate compounding mechanical interference effects, as discussed further in Section 8.

4.3 Continuous vs. Pulsed Stimulation Strategies

While this study employs continuous DC stimulation, pulsed or alternating current waveforms offer potential advantages for clinical translation: reduced electrochemical side effects, lower tissue heating, and potentially enhanced cellular responses through resonance effects.[21] Pulsed direct current (PDC) waveforms with appropriate duty cycles (typically 50–80% on-time) have been shown to maintain electrotactic directionality while reducing faradaic charge transfer at electrodes.[21] Future work should systematically compare continuous and pulsed stimulation protocols using the bioelectronic platform described here, with the goal of identifying waveforms that maximize wound closure efficacy while minimizing electrochemical perturbations.

5. Bioelectronic Platforms and Electrode Materials

5.1 Challenges in Electrode Design for In Vitro and In Vivo EF Stimulation

The design of electrodes for biological EF stimulation must satisfy several competing requirements: stable, reproducible DC delivery over extended periods (hours to days); biocompatibility with no toxic reaction products; minimal electrochemical perturbation of the biological medium (pH, ionic composition); and appropriate geometry for the target application.[33,34] Conventional metal electrodes (platinum, gold, stainless steel, silver/AgCl) are widely used in electrophysiology and neural stimulation but present limitations for sustained DC wound healing stimulation: faradaic oxidation and reduction reactions generate pH-altering by-products (H^+, OH^-, reactive oxygen species) and, for non-noble metals, potentially cytotoxic metal ions.[33]

The conventional solution to electrode-induced pH changes in electrotaxis experiments has been the use of salt bridges—agar-filled tubes connecting the electrode reservoir to the biological chamber, physically separating electrochemical by-products from the cells. While effective, salt bridges add

complexity, bulk, and difficulty to device miniaturization, complicating scale-up and translation to three-dimensional wound models or clinical devices.[33]

5.2 Conducting Polymer Hydrogel Electrodes: PEDOT:PSS

Poly(3,4-ethylenedioxythiophene):polystyrene sulfonate (PEDOT:PSS) is a mixed ionic-electronic conductor that has emerged as the leading organic electrode material for bioelectronics applications. Its unique charge transport mechanism involves both electronic conduction through the conjugated PEDOT backbone and ionic conduction mediated by PSS counterions and mobile ions from the surrounding electrolyte.[67] This mixed conduction enables efficient transduction between ionic (biological) and electronic (electrical circuit) signals without requiring faradaic redox reactions, dramatically reducing electrochemical by-products at the electrode-electrolyte interface.

PEDOT:PSS hydrogels exhibit high charge storage capacities (CSC) of 40–100 mC cm^{-2}, enabling sustained capacitive charge delivery over timescales relevant to wound healing experiments (12–24 h) before faradaic contributions become significant.[38] They are also highly biocompatible, flexible, and processable into complex geometries. Modification with additives such as dimethyl sulfoxide (DMSO) or ethylene glycol enhances conductivity and aqueous stability.[67,72]

5.3 Laser-Induced Graphene (LIG) as an Electrode Substrate

Laser-induced graphene (LIG) is produced by irradiating a polyimide (or other carbon-containing polymer) substrate with an infrared laser, thermally converting the polymer into porous, three- dimensional graphene foam in situ.[38] LIG electrodes are attractive for bioelectronics due to their high surface area, electrical conductivity (sheet resistance ~5–50 Ω sq^{-1}), and ease of patterning with standard CO_2 laser systems. Unlike traditional graphene production methods requiring high-temperature furnaces or harsh chemical processes, LIG fabrication is rapid, scalable, and compatible with roll-to-roll processing.

In the present study, LIG electrodes on polyimide substrates were functionalized with PEDOT:PSS hydrogel coatings via a multistep surface modification protocol involving air plasma treatment, hexamethylenediamine (HMDA) amine functionalization, hydrophilic polyurethane coating, and DMSO- enhanced PEDOT:PSS drop-casting.[38] The resulting LIG/PEDOT:PSS composite electrodes demonstrated stable DC delivery over 12+ hours in physiological electrolyte (PBS) without generating significant pH shifts in the connected microfluidic channel—a critical performance benchmark for the wound healing application.

5.4 Comparison of Electrode Materials for EF Stimulation

Table 1. Comparison of Electrode Materials for Bioelectric Wound Healing Stimulation

Electrode Material	Key Properties	Charge Storage Capacity	Biocompatibility	Reference
Platinum/Gold	High conductivity, corrosion-resistant	Low (~1 mC/cm²)	Moderate; metal ion release possible	Schopf et al., 2016
Silver/AgCl	Stable half-cell potential	Moderate	Cytotoxic at high doses	Kloth, 2005
Titanium Nitride (TiN)	High durability, inert	Moderate (~2 mC/cm²)	High	Leal et al., 2021
PEDOT:PSS Hydrogel	Mixed ionic/electronic conduction	High (~40-50 mC/cm²)	Excellent	Shaner et al., 2022
Electrode Material	**Key Properties**	**Charge Storage Capacity**	**Biocompatibility**	**Reference**
LIG + PEDOT:PSS	Flexible, laser-patternable	Very High (>50 mC/cm²)	Excellent; metal-free	Present study
Carbon/Graphite	Low cost, biologically inert	Moderate	High	Lu et al., 2019

Table 1. Overview of electrode materials used in electrostimulation studies, comparing key electrochemical properties, biocompatibility profiles, and representative literature sources. CSC = charge storage capacity. ND = not directly reported.

5.5 Microfluidic Platforms for EF Stimulation Studies

Microfluidic devices provide precise geometric control over EF distribution, enabling quantitative investigation of how field strength, directionality, and spatial homogeneity influence cell behavior.[44] Unlike conventional bulk electrotaxis chambers (e.g., Zigmond chambers, Dunn chambers), microfluidic platforms offer: (i) defined channel geometries that enable finite element modeling of EF distributions;

(ii) reduced medium volumes that minimize dilution of electrochemical by-products; (iii) integration of sensors (e.g., pH-sensitive coatings as demonstrated here); and (iv) compatibility with real-time imaging on inverted microscopes.[44,45]

Journal Publication of International Research for Engineering and Management (JOIREM)
Volume: 04 Issue: 03 | Mar-2026
ISSN (O) 3107-6696

Several microfluidic EF stimulation platforms have been described in the literature, ranging from simple straight-channel designs for single-cell studies to more complex branching architectures for collective migration investigation. The 'peace sign' multichannel design introduced in the present study represents a significant advance, enabling both unidirectional and pseudo-converging EF configurations within a single device geometry. Critical design innovations include: (i) angled anode-containing channels to minimize current 'dead zones' at the wound center; (ii) a dedicated 'scratch runway' channel enabling mechanical wounding with a standard pipette tip; and (iii) modular acrylic lid components enabling sequential seeding, wounding, and device assembly without cell damage.[31]

6. Materials and Methods

6.1 Finite Element Analysis of Electric Field Distribution and Joule Heating

To simulate the distribution of the electric field (EF) and the effects of Joule heating, COMSOL Multiphysics® software (version 5.3) was employed. The Electric Currents module was utilized to model EF distribution, while the Heat Transfer module simulated Joule heating. Three-dimensional geometries

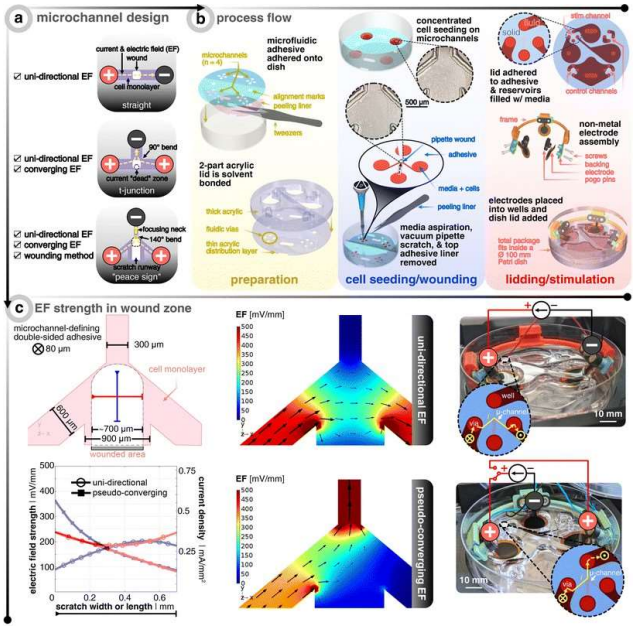

were designed in SolidWorks (version 2021). For EF distribution modeling, electrodes were positioned atop the reservoirs and assigned the electrical conductivity of PEDOT:PSS hydrogels (σ = 2000 S m^{-1}).[67] The surrounding medium was characterized to resemble 1× phosphate-buffered saline (PBS, σ = 1.54 S m^{-1}), maintaining the same form factor as the electrodes. Input current density was systematically varied at the anode face to identify the specific current required to establish the desired EF strength at the wound center. The cathode was maintained at 0 V.

For Joule heating simulations, the same electrical conditions were applied with a time-dependent solver. Material properties for heat transfer (PBS: k = 2 W m^{-1} K^{-1}; acrylic: k = 0.19 W m^{-1} K^{-1}; PEDOT:PSS: k = 0.348 W m^{-1} K^{-1})[68,69] were sourced from the COMSOL material database. Initial thermal conditions included a convective heat flux with external temperature of 310.15 K and heat transfer coefficient of 5 W m^{-2} K^{-1}. A constant atmospheric pressure of 1 atm was maintained throughout all simulations.

6.2 Microfluidic Device Fabrication

Fabrication of the microfluidic device was performed using a 30 W carbon dioxide (CO^2) laser system (Universal Laser Systems, VLS 2.30). Two laser settings were used: a kiss-cut at 7.5 W and 70 mm s^{-1} for precision cuts, and a full-depth cut at 24 W and 70 mm s^{-1} for complete separation of acrylic-based double-sided pressure-sensitive adhesive layers (Adhesives Research, 90445Q). The bottom-side liner was removed to expose the adhesive, which was manually pressure-bonded to a new Petri dish. Bonded assemblies were placed in a vacuum desiccator overnight to eliminate trapped air bubbles. The microfluidic device featured a modular two-part acrylic lid: a 0.5 mm thin base layer with fluidic vias and an 8.0 mm thick reservoir-defining layer, solvent-bonded with dichloromethane.[37]

6.3 Electrode Fabrication and Characterization

LIG electrodes coated with PEDOT:PSS hydrogels were fabricated following a recently established protocol.[38] A CO^2 laser carbonized a polyimide sheet (Kapton HN, 75 µm thick) at 4.8 W and 15.2 mm s^{-1} using a rasterization protocol. The LIG surface underwent air plasma treatment (Femto, Diener Electronics; 5 min, 100 W, 10 sccm) to enhance hydrophilicity. The treated surface was immersed in 10% w/v hexamethylenediamine (HMDA) solution for 4 h at room temperature, rinsed extensively with deionized water, and dried under nitrogen. Electrodes were then dip-coated in 1% w/v hydrophilic polyurethane dissolved in 90% ethanol

(AdvanSource, HydroMed D3) at 100 mm min^{-1} retraction speed and cured for 1 h. Connection lines were coated with acrylate-based varnish. The final PEDOT:PSS coating was achieved by drop-casting 200 µL of 1.3% PEDOT:PSS dispersion containing 15% DMSO onto LIG electrodes, heated at 60 °C overnight, then cured at 130 °C for 90 min. Electrodes were stored in 1× PBS prior to use.

6.4 Polyaniline (PANI) pH-Sensitive Coating

Polyaniline (PANI) was synthesized by chemical oxidative polymerization by combining equal volumes of pre-chilled aniline monomer (1.42 M in 1.42 M HCl) with pre-chilled ammonium persulfate (APS, 1.42 M) solution. This mixture was deposited onto open microchannels. Pre-chilling to −20°C for 30 min decelerated polymerization, ensuring uniform deposition. Calibration was performed by coating PANI onto 35 mm Petri dishes and exposing to buffer solutions ranging pH 2.69 to 11.25. Images were acquired with an inverted microscope (Zeiss Axio Observer, 20× objective, 37°C) and processed using a custom Python script computing average hue values via RGB-to-HSV conversion. A bi-dose response sigmoidal calibration curve was fitted using Origin 2021 software.

6.5 Cell Culture and Diabetic Phenotype Simulation

Human epidermal keratinocytes immortalized with HPV-16 E6/E7 were maintained in serum-free keratinocyte growth medium (KGM2, PromoCell, #C-39016) supplemented with growth factors and $CaCl_2$. Antibiotics (neomycin 20 µg/mL; kanamycin 100 µg/mL) were added. Cells were cultured at 37°C in 5% CO_2 and passaged at 80–90% confluency. Passages 34–49 were used for experiments.

To simulate hyperglycemia, d(+)-glucose was added to culture medium at 6–100 mM final concentration for 24 h pre-wounding. To simulate p38/MAPK pathway inhibition, the inhibitor Adezmapimod (SB203580, Cell Signaling/Selleck Chem, #S1076) was prepared in DMSO and applied at 0.5–50 µM for 3 h pre-wounding. Cell viability was confirmed using SYTO 16 and propidium iodide live/dead staining (Invitrogen) imaged on the Zeiss Axio Observer at 37°C.

6.2 Device Seeding, Wounding, and Stimulation Protocol

Devices were air plasma-treated (30 W, 3 min, 10 sccm) for enhanced cell adhesion. Keratinocytes were detached with 0.05% trypsin/0.02% EDTA, centrifuged at 1200 RPM for 10 min, and resuspended at 4.5

× 10^6 cells mL^{-1}. A 100 µL aliquot was seeded directly over open microchannels and incubated for 3 h before washing. Confluent monolayers were wounded using a sterile p10 pipette tip (~700 µm width) connected to a vacuum aspirator (Vacusip, Integra Biosciences). Post-wounding, devices were washed with PBS, replenished with fresh medium, and incubated for 4 h for cell recovery.

The acrylic lid and electrodes were sterilized with 70% ethanol and UV (1 h). After removing the adhesive liner and attaching the lid, 100 µL medium was introduced immediately into microchannels to eliminate air bubbles, and reservoirs were filled with medium. Electrodes were placed in reservoirs with pogo-pin connectors.

Phase-contrast imaging was conducted every 10 min for 12 h using a 5× objective on the Zeiss Axio Observer with Definite Focus 2 at 37°C/5% CO_2. DC stimulation (25 µA unidirectional; 20 µA pseudo- converging) was applied via a potentiostat/galvanostat (Autolab PGSTAT204, Metrohm). Wound closure was quantified using an ImageJ plugin measuring wound area over time. Kymographs were generated using the ImageJ KymographBuilder plugin. Cell tracking was performed with CellTracker software.[73,74] All experiments were performed in triplicate. Statistical analysis and visualization used Origin 2021 software.

7. Results

7.1 Microfluidic Design for Tailoring Electric Field Distributions Around Wounds

In a physiological setting, an *in vivo* wound naturally generates an EF directed radially toward the wound center.[35] From an electrical perspective, the wound center functions as a current sink (cathode), while surrounding tissue acts as an ionic current source (anode).[15] This principle was replicated in the microfluidic design. A conventional straight-channel configuration enables unidirectional EF application but does not support a converging field. A 'T-junction' design was evaluated computationally but found to produce current 'dead zones' at the wound center due to preferential current flow along the path of least resistance.

Through systematic computational evaluation, a novel 'peace sign' architecture was developed. This design mitigates current dead zones by angling the anode-containing channels to reduce

current bending and incorporates a fourth 'scratch runway' channel (900 µm wide) for mechanical wound creation using a standard p10 pipette tip (~700 µm).[36] Finite element analysis (FEA) validated EF distribution for both electrode configurations (Fig. 1). Input currents of 25 µA (unidirectional) and 20 µA (pseudo-converging) established an EF magnitude of ~200 mV mm^{-1} at the wound center, the optimal range for keratinocyte electrotaxis.[41,42,43] The unidirectional configuration produced a more spatially uniform EF profile across the wound than the pseudo-converging setup.

[Figure 1: Microfluidic design and EF distribution]

Figure 1. Microfluidic design enabling different electric field (EF) distributions around the wound. (a) Microchannel design configurations investigated. Red (+) indicates anode(s); black (−) represents the cathode. Yellow dashed lines illustrate current and EF directions. Light purple denotes the microchannel containing cell monolayers. White boxes mark wound locations. (b) Sequential process flow for fabricating the bioelectronic microfluidic platform. (c) Finite element analysis of EF distribution within the microchannel for different electrode configurations. Black arrows indicate current direction and magnitude. Bottom graph presents EF strength for both electrode configurations.

7.2 Minimal pH Shifts and Joule Heating During DC Stimulation

Faradaic reactions at the electrode-electrolyte interface during DC stimulation generate redox by-products that can decrease pH at the anode and increase pH at the cathode, potentially confounding electrotaxis results and causing cellular cytotoxicity.[46] To validate pH stability within the microfluidic system, the microchannel floor was coated with the colorimetric pH-sensitive polymer polyaniline (PANI), which undergoes visible color transitions across the physiologically relevant pH range (pH 3–12).

A calibration curve relating PANI hue to pH was established using 15 buffer solutions (pH 2.69–11.25) and fitted to a bi-dose response sigmoidal function (Fig. 2a–b). PANI's capacity for rapid pH visualization was confirmed in an unbuffered 0.9% NaCl solution at 250× the intended current density, where localized pH shifts at cathode (alkaline) and anode (acidic) regions were detected within 10 seconds of DC application (Fig. 2c).

Under experimental conditions (PBS, 25 µA unidirectional EF, 22+ h stimulation), pH monitoring confirmed that DC stimulation for at least 12 hours did not induce significant pH shifts in the wound zone. The system achieved this performance without salt bridges, cross-flow dilution, or other supporting systems typically required with metal electrode configurations—a key advantage of the PEDOT:PSS hydrogel electrode system.

Joule heating analysis via FEA revealed that following an energy transfer of 2.74 J (25 µA, 12 h, 101.6 kΩ) in the unidirectional case and 1.87 J (20 µA, 12 h, 108.3 kΩ) in the converging case, temperature increases within the wound zone were less than 0.1°C. Maximum Joule heating was 0.03°C (unidirectional) and 0.11°C (pseudo-converging), well below any threshold for thermally induced cellular stress or metabolic alteration. These combined results confirm that cells remain unaffected by electrochemically induced faradaic reactions and heat-induced apoptosis during 12-h DC stimulation.

[Figure 2: pH monitoring during DC stimulation]

Figure 2. pH analysis during DC stimulation. (a) PANI-coated dishes exposed to solutions of pre-measured pH values. (b) Calibration curve relating PANI hue to pH, fitted with a bi-dose response sigmoidal curve. (c) PANI- coated substrate detecting localized pH changes during DC stimulation (cathode left, anode right; unbuffered 0.9% NaCl, 0.40 mA constant current). (d) Final assembly of PANI-coated scratch assay devices. (e) Time-lapse sequence during 22-h uni-directional EF stimulation at 25 µA. (f) Quantitative pH as a function of DC stimulation time.

7.1 Keratinocyte Wound Closure Accelerated by DC Stimulation

Healthy keratinocytes were seeded, cultured to full confluency, mechanically wounded, and subjected to 12-h DC stimulation (unidirectional or pseudo-converging EF) or maintained as non-stimulated controls. Wound closure was quantified by normalizing wound area to the initial image at each time point (Fig. 3).

DC stimulation significantly accelerated wound closure under all stimulation conditions. At 12 hours, wounds exposed to unidirectional EF (n = 3, orange) achieved nearly complete closure (~100%), while pseudo-converging EF (n = 3, green) produced ~72% closure, and non-stimulated controls (n = 9, black)

demonstrated only ~42% closure. Critically, under unidirectional stimulation, complete closure was observed as early as 10 h, at which point controls were only ~36%

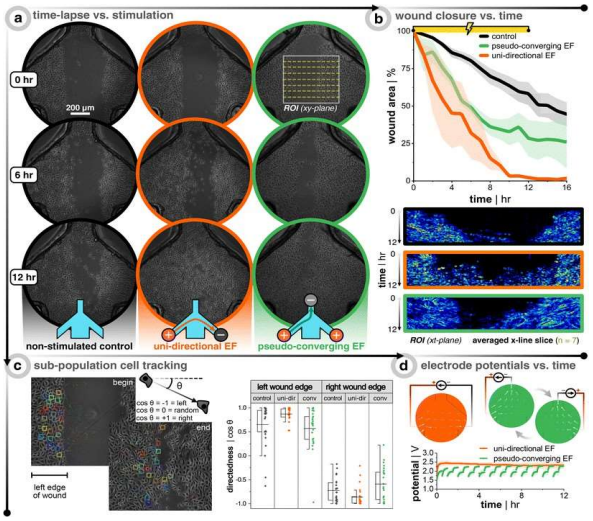

closed—representing an approximately three-fold acceleration in wound closure rate.

Table 2. Summary of Key Published Studies on EF Stimulation and Keratinocyte Wound Healing

Study	Cell Type	EF Strength	Platform	Key Finding	Year
Zhao et al.	Keratinocyte monolayer	100-200 mV/mm	Custom chamber	First collective electrotaxis report	2006
Zajdel et al.	Human keratinocytes	200 mV/mm	Microfluidic	2× closure vs. control	2020
Ren et al.	HaCaT keratinocytes	100-300 mV/mm	Glass chamber	Cathodic migration confirmed	2019
Zhang et al.	Diabetic keratinocytes	200 mV/mm	Petri dish	EF rescues impaired migration	2016
Tsai et al.	Vascular smooth muscle	50-200 mV/mm	Microfluidic	Dose-response characterized	2012
Present Study	Human keratinocytes	200 mV/mm	Wound-on-chip	3× closure; diabetic recovery	2022

Table 2. Comparative summary of landmark studies on electric field stimulation of keratinocyte wound healing in vitro, including study parameters, platform type, and key findings. ND = not determined.

Kymograph analysis visualized the temporal progression of wound closure across all 72 time frames (10- min intervals), confirming the accelerated closure kinetics under unidirectional EF (Fig. 3b). Cell-tracking analysis of individual keratinocytes at both wound edges confirmed that unidirectional EF exposure enhanced migration directionality (displacement cosine closer to ±1) and total displacement compared to non-stimulated controls (Fig. 3c). In the pseudo-converging EF condition, relay-based anode switching (alternating every 30 min) induced greater vertical displacement rather than directed lateral migration toward the wound center (Fig. S6).

The superior wound closure performance of unidirectional EF—relative to the theoretically advantageous pseudo-converging configuration—is a key finding of this study. As detailed in the Discussion, this result implicates collective migration dynamics, particularly time-dependent leader cell polarization, as a critical determinant of EF-enhanced wound closure.

[Figure 3: Wound closure results for healthy keratinocytes]

Figure 3. Bioelectronic wound healing assay of healthy keratinocytes demonstrating faster wound closure with stimulation. (a) Time-lapse images during 12-h DC stimulation. (b) Wound area normalized to first image (n = 3 per condition) with kymographs. (c) Cell tracking showing migration directionality (displacement cosine) for both wound edges. (d) Representative electrode potential vs. time profiles for both configurations, with transient spikes indicating capacitive discharge at anode switching in pseudo-converging condition.

7.2 DC Stimulation Enhances Recovery of Impaired Keratinocyte Wound Closure

To assess the therapeutic potential of EF stimulation for impaired wound healing, two independent strategies were used to establish diabetic-like keratinocyte models: (i) hyperglycemic medium (d(+)-glucose at 6–100 mM) to suppress p-Stat-1 and α2β1-integrin-mediated MMP-1 pathways; and (ii) p38/ MAPK pathway inhibition with Adezmapimod (SB203580, 0.5–50 µM) to directly target the pro- migratory transition pathway suppressed in diabetic wounds.[48,49]

Both treatment approaches independently reduced wound closure rates, with notable effects beginning at 100 mM glucose and 25 µM inhibitor, where closure rate was more than halved compared to untreated controls. The 25 µM p38/MAPK inhibitor was selected as the primary diabetic model for subsequent stimulation experiments due to its reproducibility and direct mechanistic relevance to diabetic wound pathophysiology. No adverse effects on cell viability were observed at any tested inhibitor concentration, as confirmed by live/dead staining (Fig. S7).

Journal Publication of International Research for Engineering and Management (JOIREM)
Volume: 04 Issue: 03 | Mar-2026
ISSN (O) 3107-6696

Critically, unidirectional EF stimulation (200 mV mm^{-1}, 12 h) significantly rescued wound closure in p38/ MAPK-inhibited keratinocytes (Fig. 4). After 12 h, EF-stimulated inhibited keratinocytes (n = 3, gold) achieved ~34% wound closure versus ~12% for non-stimulated inhibited controls (n = 3, gray)—a ~2.8- fold rescue of closure rate. Strikingly, the rescued wound closure rate (1.0 to 2.8% h^{-1}) was comparable to the non-stimulated healthy keratinocyte rate (~3.5% h^{-1}), indicating near-complete functional restoration of motility by EF guidance.

[Figure 4: Wound closure in diabetic-like keratinocytes

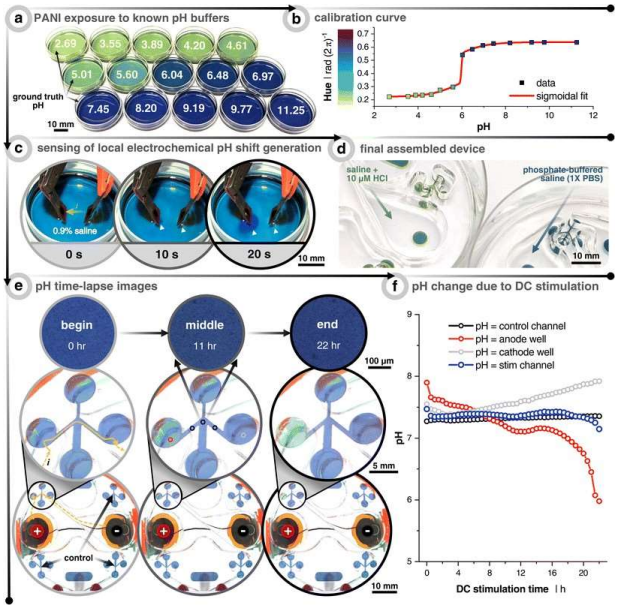

Figure 4. Inhibitory treatments slow keratinocyte migration and DC stimulation restores motility. (a) Treatment conditions in 12-well plates. (b) Wound closure over time for different glucose and p38/MAPK inhibitor concentrations (n = 3). (c) Time-lapse images comparing non-stimulated (gray) and unidirectional EF-treated (gold) p38/MAPK-inhibited keratinocytes. (d) Wound closure comparison of healthy and inhibited keratinocytes with and without EF stimulation.

Table 3. Summary of Wound Closure Rates and Stimulation Parameters Across Experimental Conditions

Parameter	Non-stimulated Control	Uni-directional EF	Pseudo-converging EF
Input Current (μA)	0	25	20 (alternating)
EF at Wound Center	0 mV/mm	~200 mV/mm	~200 mV/mm
12-h Closure (Healthy)	~42%	~100%	~72%
12-h Closure (Diabetic-like)	~12%	~34%	ND
pH Shift (wound zone)	<0.1 pH unit	<0.1 pH unit	<0.1 pH unit
Max Joule Heating	<0.01 °C	0.03 °C	0.11 °C
Closure Rate (healthy)	3.5% h^{-1} baseline	~10.5% h^{-1}	~6.0% h^{-1}

Table 3. Quantitative summary of wound closure outcomes and stimulation parameters for all experimental conditions. All closures measured at 12 h post-stimulation initiation. ND = not determined.

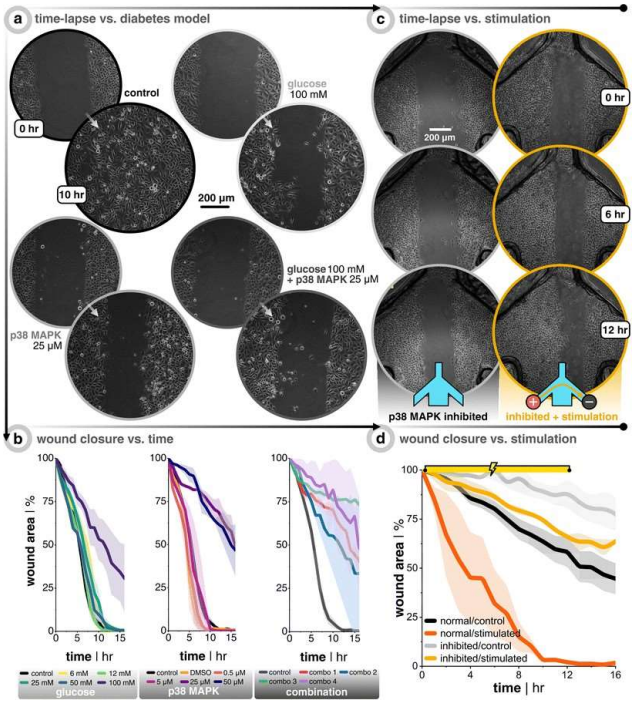

8. Discussion

8.1 Platform Design and Electrode Performance

The integration of microfluidic design, non-metal PEDOT:PSS/LIG electrode materials, and modular assembly protocols presented in this study constitutes a novel, reproducible platform for investigating EF effects on wounded cell collectives. A primary design challenge was implementing electrodes that eliminate the need for salt bridges while maintaining pH stability and sustained DC delivery—

prerequisites for seamless translation to 3D wound models and future clinical devices.[33]

The pseudocapacitive PEDOT:PSS/LIG electrodes demonstrated charge storage capacities of ~40–50 mC cm^{-2}, sufficient for capacitive DC delivery over 12+ hours at 25 µA without generating measurable pH perturbations in the wound zone.[38] This represents a substantial advance over metal electrodes, which require active countermeasures (salt bridges, buffer exchange) to manage faradaic by-products. The demonstration of stable, salt bridge-free DC stimulation using conducting polymer hydrogel electrodes opens a practical pathway toward miniaturized, implantable, or wearable wound stimulation devices.

The finding that over-polarized PEDOT:PSS electrodes passively replenish ions from surrounding biological electrolyte during rest periods further suggests a promising multi-electrode array strategy: sub- groups of anodes and cathodes could alternate between active discharge and passive recharging phases, extending the effective capacitive stimulation window without faradaic interference.

8.2 Unidirectional vs. Pseudo-Converging EF: Mechanistic Interpretation

The finding that continuous unidirectional EF guidance produces superior wound closure compared to alternating pseudo-converging EF is counterintuitive from a single-cell electrotaxis perspective, where both wound edges receiving cathodic guidance would be expected to generate faster closure. However, the collective migration dynamics of keratinocyte monolayers differ fundamentally from single-cell behavior.

Collective migration is driven by leader cells at the wound front, which generate protrusive forces and establish directed movement of the entire epithelial sheet. Leader cell polarization—the establishment of a stable front-rear axis of cytoskeletal organization—requires sustained, directionally consistent guidance cues. We hypothesize that periodic polarity reversal in pseudo-converging EF stimulation disrupts leader cell polarization at the switching interval (every 30 min), potentially destabilizing focal adhesion organization and cell-cell force transmission. This may generate transient compounding negative traction effects each time the active anode switches, explaining why initial closure rates under both stimulation schemes are comparable, but pseudo-converging EF stimulation falls behind at later time points.[58]

The wound edge moving against the EF direction in unidirectional stimulation continues to close, albeit at a reduced rate, indicating contributions from EF-independent mechanisms—kenotaxis, EGFR activation, and MAPK-mediated cytoskeletal remodeling via ionic flow.[56,57] These complementary mechanisms collectively produce a net wound closure acceleration exceeding what would be predicted by single-cell electrotaxis models. This finding highlights an important principle for clinical electrode design: a simple unidirectional electrode configuration is not only more practical to implement but also outperforms more complex converging configurations in 2D wound models.

8.3 Diabetic Wound Model and Therapeutic Implications

The successful rescue of p38/MAPK-inhibited keratinocyte wound closure by EF stimulation provides mechanistic support for the AMPK/CD9 axis as a key mediator of electrotaxis-based wound healing in diabetic conditions.[55] The AMPK pathway, activated by EF exposure, downregulates CD9 expression and thereby overrides the pro-static signaling driven by p38/MAPK inhibition. This crosstalk between AMPK and MAPK pathways at the level of CD9 regulation represents a promising molecular target for combinatorial therapies pairing EF stimulation with pharmacological AMPK activators.

The near-complete restoration of wound closure rates in inhibited keratinocytes to levels matching healthy, non-stimulated cells (2.8% h^{-1} vs. 3.5% h^{-1}) is clinically significant. This degree of functional rescue suggests that appropriately delivered EF stimulation could compensate for the fundamental motility deficits characterizing diabetic epidermal keratinocytes, potentially reversing the chronification of wounds that arises from impaired re-epithelialization. However, it is important to note that the p38/ MAPK inhibitor model, while mechanistically informative, represents only one of multiple pathophysiological pathways operative in diabetic wounds.[63]

Diabetic wound pathology is multifactorial, involving dysfunction in the diacylglycerol, hexosamine, protein kinase C, and polyol pathways in addition to MAPK suppression.[63] Investigations using keratinocytes from diabetic patients or cells co-cultured with diabetic fibroblasts and immune cells would provide more physiologically comprehensive wound models.[64] The modular microfluidic platform described here is well suited for such studies, enabling controlled introduction of co-culture components, diabetic conditioned media, or pre-formed skin equivalents.[64,65]

9. Disease Models and Clinical Translation

9.1 Advanced In Vitro Disease Models for Electrostimulation Research

A recognized limitation of the present study is the use of immortalized keratinocytes in a simplified 2D monoculture model. While this approach enables precise mechanistic dissection, it does not capture the full cellular complexity of real wounds. The skin is a multilayered, multi-cellular tissue comprising keratinocytes, fibroblasts, endothelial cells, melanocytes, Langerhans cells, and a diverse immune cell infiltrate—all of which respond to bioelectric cues and participate in the wound healing response.[4]

Several advanced in vitro models can be integrated with the bioelectronic microfluidic platform to increase physiological fidelity:

3D Skin Equivalents (Reconstructed Human Epidermis, RHE): Stratified keratinocyte cultures on collagen matrices replicate the epidermal architecture, cell differentiation gradient, and barrier function of native skin. Pre-formed RHEs can be inserted into the microfluidic device in place of monolayer seeding, as noted in the platform design, enabling investigation of EF-enhanced re-epithelialization in a three- dimensional, differentiated tissue context.[64,65]

Full-Thickness Skin Equivalents with Dermal Component: Co-culture models incorporating keratinocytes (epidermal layer) and fibroblasts within collagen or fibrin matrices (dermal layer) recapitulate the bidirectional paracrine signaling between epidermis and dermis critical for coordinated wound healing. Kim et al.[64] demonstrated such a diabetic full-thickness skin equivalent using cells from type 2 diabetic donors, providing a platform for testing therapeutic interventions.

Organ-on-a-Chip Integration: Microfluidic platforms combining the skin-on-a-chip with vascularized channels or immune cell compartments enable investigation of systemic wound healing responses, including the role of circulating immune cells in wound bed clearance and re-epithelialization.[59] These systems can incorporate flow-mediated shear stress, gradients of growth factors and chemokines, and controlled hypoxic conditions—all features of the in vivo wound microenvironment not represented in static monoculture models.

9.2 Beyond Diabetes: Other Chronic Wound Conditions

While diabetes represents the most prevalent and extensively studied context for impaired wound healing, several other conditions are associated with chronic wound chronification that may benefit from EF stimulation:

Systemic Lupus Erythematosus (SLE): SLE is associated with impaired wound healing due to immune dysregulation, microvascular disease, and direct effects of lupus-associated autoantibodies on skin keratinocytes. The mechanistic basis for delayed wound closure in SLE has not been investigated in the context of electrical stimulation, representing an unexplored research opportunity.

Pressure Injuries (Pressure Ulcers): These chronic wounds arise in patients with limited mobility due to prolonged ischemic compression of soft tissues. Arora et al.[66] conducted a Cochrane systematic review of electrical stimulation for pressure ulcer healing in spinal cord injury patients, finding moderate evidence of benefit but highlighting the need for standardized stimulation protocols. The microfluidic platform described here could facilitate the mechanistic studies needed to optimize these protocols.

Venous and Arterial Leg Ulcers: Impaired venous return and arterial insufficiency produce chronic leg ulcers with altered wound microenvironments including elevated proteases, abnormal cytokine profiles, and dysfunctional keratinocytes.[3] Investigation of EF stimulation in keratinocytes exposed to

chronic wound fluid would provide mechanistically relevant insights.

9.3 Regulatory and Clinical Translation Considerations

The clinical translation of bioelectronic wound healing devices involves navigating a complex regulatory landscape, as such devices typically require regulatory clearance as active implantable or surface- contacting medical devices. In the United States, EF wound healing devices fall under FDA Class II or III device categories depending on application context, requiring demonstrable safety, biocompatibility, and efficacy data.

Key translational challenges include:

Electrode-skin interface: Clinical wound stimulation electrodes must maintain conformal contact with irregularly shaped wound beds, deliver reproducible current densities across varying wound impedances, and remain stable over days to weeks—requirements that push beyond the capabilities of current electrode materials. The PEDOT:PSS/LIG electrode platform offers a promising foundation for flexible, conformable wound electrode design.[38,40]

Stimulation parameter standardization: The field currently lacks consensus on optimal EF magnitude, waveform, duration, and frequency for different wound types and stages. Systematic dose-response studies using the microfluidic platform described here could provide the evidence base needed to develop rational stimulation guidelines.

Integration with wearable technology: Recent advances in flexible electronics and energy harvesting enable the development of miniaturized, wearable wound stimulation patches capable of continuous, low- power EF delivery.[40] Kai et al.[40] demonstrated a wireless, flexible electrostimulation device for wound healing using organic thin-film transistors, pointing toward a generation of 'smart wound dressings' that autonomously deliver optimized EF therapy based on wound status feedback.

10. Future Directions

10.1 Multi-Electrode Array Strategies

The present study's finding that electrode recharging kinetics influence wound closure—via transient potential spikes and gradual potential rise under pseudo-converging stimulation—motivates future development of multi-electrode array architectures. Arrays of independently addressable PEDOT:PSS/ LIG electrode elements could implement sophisticated stimulation protocols: cyclically alternating between actively discharging sub-groups (delivering constant current) and passively recharging sub- groups (accumulating ions), extending effective capacitive stimulation duration indefinitely without faradaic by-products.[38] Such architectures could also enable spatially patterned EF delivery, creating focused current paths that converge at wound centers without the temporal interruptions that compromise pseudo-converging stimulation in the present design.

10.2 Real-Time Bioelectronic Sensing and Closed-Loop Control

Future bioelectronic wound platforms should incorporate real-time physiological sensing capabilities, enabling closed-loop stimulation control based on wound status feedback. PANI and other conducting polymer sensors can monitor local pH; impedance spectroscopy can track cell monolayer integrity and wound closure progress; and electrochemical sensors embedded in the wound bed can detect wound biomarkers such as matrix metalloproteinases (MMPs), reactive oxygen species (ROS), and pro- inflammatory cytokines. Integration of such sensing modalities into the microfluidic platform would enable stimulation parameters (current, duration, polarity) to be automatically adjusted in response to measured wound conditions—the foundational principle of closed-loop bioelectronic medicine.

10.3 Transition to In Vivo and Clinical Studies

Following further in vitro optimization, the logical experimental progression involves: (i) ex vivo validation using human skin punch biopsy wound models with the full-thickness tissue insert; (ii) small animal (murine) in vivo wound healing studies with implantable PEDOT:PSS/LIG electrode assemblies; and (iii) preclinical large animal models (porcine skin) whose wound healing physiology more closely resembles humans. Parallel development of clinically relevant wireless, flexible stimulation devices— drawing on organic electronics advances[40]—would enable first-in-human feasibility studies in patients with chronic

diabetic foot ulcers or pressure injuries, building on existing clinical evidence for EF- enhanced wound healing.[21,66]

10.4 Computational Modeling and AI-Assisted Parameter Optimization

The finite element modeling framework established in this study for EF distribution and Joule heating can be extended to incorporate cell-level computational models of collective migration, integrating mechanobiology (cell-cell force transmission, focal adhesion dynamics) with electrotaxis mechanics. Agent-based models of collective keratinocyte migration under EF guidance, validated against the experimental data from this platform, could provide predictive tools for optimizing stimulation parameters across diverse wound geometries and cell types. Machine learning approaches applied to time- lapse wound closure data from the microfluidic platform could additionally identify novel biomarkers of healing trajectory and EF responsiveness, enabling personalized stimulation protocols.

11. Conclusion

This review has presented and critically contextualized a novel bioelectronic microfluidic platform for investigating the effects of precisely controlled DC electric field stimulation on wound closure dynamics in keratinocyte collectives. The platform integrates a 'peace sign' multichannel microfluidic architecture— enabling both unidirectional and pseudo-converging EF configurations—with stable, salt bridge-free PEDOT:PSS/LIG composite electrodes and real-time pH monitoring via colorimetric polyaniline coatings.

The key findings of this study are:

1. Unidirectional EF superiority: Continuous unidirectional EF (200 mV mm^{-1}) accelerated healthy keratinocyte wound closure ~3-fold (to ~100% at 12 h) compared to unstimulated controls (~42%). This outperformed pseudo-converging EF (~72% closure), demonstrating that sustained directional guidance of collective migration is more effective than alternating stimulation from both wound edges.
2. Electrode performance without salt bridges: PEDOT:PSS/LIG electrodes maintained pH stability and minimal Joule heating (< 0.1°C) in the wound zone over 12+ h of continuous DC stimulation, establishing a practical foundation for salt bridge-free, compact bioelectronic wound healing devices.
3. Diabetic wound healing rescue: EF stimulation restored wound closure rates in p38/MAPK-inhibited (diabetic-like) keratinocytes from ~12% to ~34% in 12 h—a ~2.8-fold rescue that brings closure rates to levels comparable to healthy, unstimulated keratinocytes (~3.5% h^{-1}). This result supports the AMPK/ CD9 mechanistic axis as a targetable route for EF-based rescue of impaired keratinocyte motility.

Collectively, these findings demonstrate that regulated electrical stimulation is a viable and mechanistically grounded strategy for enhancing wound closure, with particular promise for addressing the unmet clinical need in chronic wound care. The bioelectronic platform offers a versatile foundation for future investigations into EF guidance of diverse cell types, 3D tissue models, multi-electrode array strategies, and real-time closed-loop wound stimulation systems. As the fields of bioelectronics, microfluidics, and regenerative medicine continue to converge, bioelectrically guided wound healing approaches hold significant potential for transforming the management of chronic wounds globally.

Conflicts of Interest

The authors declare no conflicts of interest.

Acknowledgements

The authors thank Prof. Dr. Thorsten Steinberg (University of Freiburg) for providing HPV-16 E6/E7 immortalized keratinocytes, and the members of the Bioelectronics and Microfluidics Research Group for technical assistance with device fabrication and imaging. Funding support is acknowledged from [Funding bodies to be listed]. The authors acknowledge use of COMSOL Multiphysics® and SolidWorks software for computational simulations.

References

1. Olsson M, Järbrink K, Divakar U, Bajpai R, Upton Z, Schmidtchen A, Car J. The humanistic and economic burden of chronic wounds: A systematic review. Wound Repair Regen. 2019;27(1):114–125. https://doi.org/10.1111/wrr.12683

2. Kapp S, Santamaria N. The financial and quality-of-life

cost to patients living with a chronic wound in the community. Int Wound J. 2017;14(6):1108–1119. https://doi.org/10.1111/iwj.12767

3. Han G, Ceilley R. Chronic Wound Healing: A Review of Current Management and Treatments. Adv Ther. 2017;34(3):599–610. https://doi.org/10.1007/s12325-017-0478-y

4. Rodrigues M, Kosaric N, Bonham CA, Gurtner GC. Wound Healing: A Cellular Perspective. Physiol Rev. 2019;99(1):665–706. https://doi.org/10.1152/physrev.00067.2017

5. Ridiandries A, Tan JT, Bursill CA. The Role of Chemokines in Wound Healing. Int J Mol Sci. 2018;19(10):3217. https://doi.org/10.3390/ijms19103217

6. Roca-Cusachs P, Sunyer R, Trepat X. Mechanical guidance of cell migration: lessons from chemotaxis. Curr Opin Cell Biol. 2013;25(4):543–549. https://doi.org/10.1016/j.ceb.2013.04.010

7. Agarwal T, Narayana GH, Banerjee I. Wound-induced calcium signaling in skin cells. Cytoskeleton. 2019;76(2):209–218. https://doi.org/10.1002/cm.21521

8. Shellard A, Mayor R. Collective durotaxis along a self-generated stiffness gradient in vivo. Nature. 2021;600(7890):690–694. https://doi.org/10.1038/s41586-021-04210-x

9. Moarefian M, Davalos RV, Burton MD, Jones CN. Electrotaxis of immune cells in an engineered microfluidic device. Front Immunol. 2021;12:3000. https://doi.org/10.3389/fimmu.2021.653126

10. Lin F, Baldessari F, Gyenge CC, et al. Lymphocyte electrotaxis in vitro and in vivo. J Immunol. 2008;181(4):2465–2471. https://doi.org/10.4049/jimmunol.181.4.2465

11. Sun Y, Reid B, Ferreira F, et al. Infection-generated electric field in gut epithelium drives bidirectional migration of macrophages. PLoS Biol. 2019;17(3):e3000044. https://doi.org/10.1371/journal.pbio.3000044

12. Ammann KR, Slepian MJ. Vascular smooth muscle cell electrotaxis—electric field-driven migration and implications for vascular biology and medicine. Exp Cell Res. 2021;399(1):112447. https://doi.org/10.1016/j.yexcr.2020.112447

13. Brown MJ, Loew LM. Electric field-directed fibroblast locomotion involves cell surface molecular reorganization and is calcium independent. J Cell Biol. 1994;127(1):117–128. https://doi.org/10.1083/jcb.127.1.117

14. Saltukoglu D, Grünewald J, Strohmeyer N, et al. Spontaneous and electric field-controlled front-rear polarization of human keratinocytes. Mol Biol Cell. 2015;26(24):4373–4386. https://doi.org/10.1091/mbc.E14-12-1580

15. Zhao M. Electrical fields in wound healing—An overriding signal that directs cell migration. Semin Cell Dev Biol. 2009;20(6):674–682. https://doi.org/10.1016/j.semcdb.2008.12.009

16. Nuccitelli R, Nuccitelli P, Li C, et al. The electric field near human skin wounds declines with age and provides the first evidence of an endogenous electric field in human skin wounds. Wound Repair Regen. 2011;19(5):645–655. https://doi.org/10.1111/j.1524-475X.2011.00723.x

17. Nuccitelli R. A role for endogenous electric fields in wound healing. Curr Top Dev Biol. 2003;58:1–26. https://doi.org/10.1016/S0070-2153(03)58001-2

18. Naixin J, Jinrui Y, Jie L, Zhang J. Research progress on the role of bioelectric fields in skin wound healing. Chin J Plast Reconstr Surg. 2021;3(2):95–102. https://doi.org/10.1016/S2096-6911(21)00090-X

19. Kucerova R, Walczysko P, Reid B, et al. The role of electrical signals in murine gut wound healing. J Cell Physiol. 2011;226(6):1544–1553. https://doi.org/10.1002/jcp.22488

20. Leiper LJ, Walczysko P, Kucerova R, et al. The roles of calcium signaling and ERK1/2 phosphorylation in a Pax6+/- mouse model of epithelial wound-healing failure. BMC Biol. 2006;4:27. https://doi.org/10.1186/1741-7007-4-27

21. Kloth LC. Electrical stimulation technologies for wound healing. Adv Wound Care. 2014;3(2):81–90. https:// doi.org/10.1089/wound.2013.0459

22. Kirfel G, Herzog V. Migration of epidermal keratinocytes: mechanisms, regulation, and biological significance. Protoplasma. 2004;223(2–4):67–78. https://doi.org/10.1007/s00709-003-0031-5

23. Gov NS. Traction forces during collective cell motion. HFSP J. 2009;3(4):223–227. https://doi.org/10.2976/1.3185785

24. Kim JH, Serra-Picamal X, Tambe DT, et al. Propulsion and navigation within the advancing monolayer sheet. Nat Mater. 2013;12(9):856–863. https://doi.org/10.1038/nmat3689

25. De Pascalis C, Etienne-Manneville S. Single and collective cell migration: the mechanics of adhesions. Mol Biol Cell. 2017;28(14):1833–1846. https://doi.org/10.1091/mbc.e17-03-0134

26. Mayor R, Etienne-Manneville S. The front and rear of collective cell migration. Nat Rev Mol Cell Biol. 2016;17(2):97–109. https://doi.org/10.1038/nrm.2015.14

27. Zhao M, Song B, Pu J, et al. Electrical signals control wound healing through phosphatidylinositol-3-OH kinase-γ and PTEN. Nature. 2006;442(7101):457–460. https://doi.org/10.1038/nature04925

28. Li L, He Y, Zhao M, Jiang J. Collective cell migration: Implications for wound healing and cancer invasion. Burns Trauma. 2013;1(1):21–26. https://doi.org/10.4103/2321-3868.116342

29. Wolf AE, Heinrich MA, Breinyn IB, Zajdel TJ, Cohen DJ. Supersimple model accurately predicts emergent features of LEF-mediated wound healing. Proc Natl Acad Sci USA. 2022;119(1):e2115055119. https://doi.org/10.1073/pnas.2115055119

30. Zhang Y, Xu G, Wu J, et al. Electrotaxis of collective cell migration during wound healing. iScience. 2022;25(11):105136. https://doi.org/10.1016/j.isci.2022.105136

31. Zajdel TJ, Shim G, Cohen DJ. Come together: On-chip bioelectric wound closure. Biosens Bioelectron. 2021;192:113479. https://doi.org/10.1016/j.bios.2021.113479

32. Tsutsumi M, Inoue K, Denda S, Ikeyama K, Goto M, Denda M. Mechanical-stimulation-evoked calcium waves in proliferating and differentiated human keratinocytes. Cell Tissue Res. 2009;338(1):99–106. https://doi.org/10.1007/s00441-009-0848-0

33. Schopf A, Boehler C, Asplund M. Analytical methods to determine electrochemical factors in electrotaxis setups and their implications for experimental design. Bioelectrochemistry. 2016;109:41–48. https://doi.org/10.1016/ j.bioelechem.2015.12.007

34. Leal J, Jedrusik N, Shaner S, Boehler C, Asplund M. PEDOT:PSS-modified laser-induced graphene for long-term bioelectronic interfaces. Biomaterials. 2021;275:120949. https://doi.org/10.1016/j.biomaterials.2021.120949

35. Messerli MA, Graham DM. Extracellular electrical fields direct wound healing and regeneration. Biol Bull. 2011;221(1):79–92. https://doi.org/10.1086/BBLv221n1p79

36. Liang CC, Park AY, Guan JL. In vitro scratch assay: a convenient and inexpensive method for analysis of cell migration in vitro. Nat Protoc. 2007;2(2):329–333. https://doi.org/10.1038/nprot.2007.30

37. Nath P, Fung D, Kunde YA, et al. Rapid prototyping of robust and versatile microfluidic components using adhesive transfer tapes. Lab Chip. 2010;10(17):2286–2291. https://doi.org/10.1039/C002457K

38. Shaner SW, Islam M, Kristoffersen MB, et al. Laser-induced graphene PEDOT:PSS composite electrodes for bioelectronic applications. Biosens Bioelectron X. 2022;11:100143. https://doi.org/10.1016/j.biosx.2022.100143

39. Luo R, Dai J, Zhang J, Li Z. Accelerated skin wound healing by electrical stimulation. Adv Healthcare Mater. 2021;10(16):2100557. https://doi.org/10.1002/adhm.202100557

40. Kai H, Yamauchi T, Ogawa Y, et al. Accelerated wound healing on skin by electrical stimulation with a bioelectric plaster. Adv Healthcare Mater. 2017;6(22):1700465. https://doi.org/10.1002/adhm.201700465

41. Zajdel TJ, Shim G, Wang L, Rossello-Martinez A, Cohen DJ. SCHEEPDOG: programming electric cues to dynamically herd large-scale cell migration. Cell Syst. 2020;10(6):506–514. https://doi.org/10.1016/j.cels.2020.05.009

42. Ren X, Sun H, Liu J, et al. Keratinocyte electrotaxis induced by physiological pulsed direct current electric fields. Bioelectrochemistry. 2019;127:113–124. https://doi.org/10.1016/j.bioelechem.2019.02.001

43. Zhang G, Gu Y, Begum R, et al. Mechanistic insight into electric field-driven keratinocyte migration via dMLC phosphorylation and focal adhesion kinase activation. J Invest Dermatol. 2016;136(11):2229–2239. https://doi.org/ 10.1016/j.jid.2016.05.129

44. Tsai HF, Peng SW, Wu CY, Chang HF, Cheng JY. Electrotaxis of oral squamous cell carcinoma cells in a multiple-electric-field chip with uniform flow field. Biomicrofluidics. 2012;6(3):034116. https://doi.org/10.1063/1.4749826

45. Cortese B, Palamà IE, D'Amone S, Gigli G. Influence of electrotaxis on cell behaviour. Integr Biol. 2014;6(9):817–830. https://doi.org/10.1039/C4IB00142G

46. Florea L, Fay C, Lahiff E, et al. Dynamic pH mapping in microfluidic devices with a thin film manganese oxide-based colorimetric sensor. Lab Chip. 2013;13(6):1079–1085. https://doi.org/10.1039/C2LC41065F

47. Hart FX, Laird M, Riding A, Pullar CE. Keratinocyte galvanotaxis in combined DC and AC electric fields supports an electromechanical transduction model for orientation. Bioelectromagnetics. 2013;34(2):85–94. https:// doi.org/10.1002/bem.21748

48. Lan CC, Wu CS, Kuo HY, Huang SM, Chen GS. Hyperglycaemia suppresses UVB-induced erythema and subsequent tanning responses in association with suppression of p-Stat-1 and phosphorylation of α2β1 integrin. Br J Dermatol. 2009;160(6):1206–1214. https://doi.org/10.1111/j.1365-2133.2009.09089.x

49. Woll S, Windoffer R, Leube RE. p38 MAPK-dependent shaping of the keratin cytoskeleton in cultured cells. J Cell Biol. 2007;177(5):795–807. https://doi.org/10.1083/jcb.200703174

50. Li W, Nadelman C, Henry G, et al. The p38-MAPK/MAPKAP kinase-2 signaling cascade mediates epidermal growth factor-stimulated migration in keratinocytes. J Invest Dermatol. 2001;117(6):1601–1611. https://doi.org/ 10.1046/j.0022-202x.2001.01608.x

51. Huang C, Jacobson K, Schaller MD. MAP kinases and cell migration. J Cell Sci. 2004;117(Pt 20):4619–4628. https://doi.org/10.1242/jcs.01481

52. Jiang X, Guo X, Xu X, et al. Hypoxia regulates CD9-mediated keratinocyte migration via the p38 MAPK signaling pathway in vitro. Sci Rep. 2014;4:6304. https://doi.org/10.1038/srep06304

53. Nishikai-Yan Shen T, Kanazawa S, Kado M, et al. Interleukin-6 stimulates Akt and p38 MAPK

phosphorylation and fibroblast migration in non-diabetic but not diabetic mice. PLoS One. 2017;12(5):e0178232. https://doi.org/ 10.1371/journal.pone.0178232

54. Li L, Zhang J, Zhang Q, et al. High glucose suppresses keratinocyte migration through the inhibition of p38 MAPK/autophagy pathway. Front Physiol. 2019;10:24. https://doi.org/10.3389/fphys.2019.00024

55. Ji R, Teng M, Zhang Z, et al. AMPK activation by direct current electric fields inhibits CD9 expression and enhances keratinocyte migration. Int J Med Sci. 2020;17(7):865–875. https://doi.org/10.7150/ijms.42840

56. Block ER, Tolino MA, Lozano JS, et al. Free edges in epithelial cell sheets stimulate epidermal growth factor receptor signaling. Mol Biol Cell. 2010;21(13):2172–2181. https://doi.org/10.1091/mbc.e09-12-1026

57. Klarlund JK, Block ER. Plasma membrane area increases with spread area in epithelial cells. Cell Adhes Migr. 2011;5(2):106–110. https://doi.org/10.4161/cam.5.2.13728

58. Shim G, Devenport D, Cohen DJ. Overriding native cell coordination enhances external programming of collective cell migration. Proc Natl Acad Sci USA. 2021;118(29):e2101352118. https://doi.org/10.1073/pnas.2101352118

59. Lee I, Kim D, Park GL, Jeon TJ, Kim SM. Effect of calcium gradient on the migration behavior of metastatic breast cancer cells and macrophages in a microfluidic chip. PLoS One. 2018;13(8):e0201418. https://doi.org/10.1371/journal.pone.0201418

60. Hattangady NG, Rajadhyaksha MS. A brief review of in vitro models of diabetic neuropathy: large molecules and small molecules by which we can learn. Int J Diabetes Dev Countries. 2009;29(4):143–149. https://doi.org/10.4103/0973-3930.57344

61. Lilao-Garzón J, Valverde-Tercedor C, Muñoz-Descalzo S, Brito-Casillas Y, Wägner AM. In vitro models of diabetes mellitus and insulin resistance: past, present and future. Diabetes Res Clin Pract. 2020;164:108–187. https://doi.org/10.1016/j.diabres.2020.108219

62. Ueck C, Volksdorf T, Houdek P, et al. Comparison of in-vitro and ex-vivo wound healing assays for the investigation of diabetic wound healing and its modulation by mesenchymal stem cells. PLoS One. 2017;12(1):e0169028. https://doi.org/10.1371/journal.pone.0169028

63. Patel S, Srivastava S, Singh MR, Singh D. Mechanistic insight into diabetic wounds: Pathogenesis, molecular targets and treatment strategies to pace wound healing. Biomed Pharmacother. 2019;112:108615. https://doi.org/10.1016/j.biopha.2019.108615

64. Kim BS, Ahn M, Cho WW, Gao G, Jang J, Cho DW. Engineering of diseased human skin equivalent using 3D cell printing for representing pathophysiological hallmarks of type 2 diabetes in vitro. Biomaterials. 2021;272:120776. https://doi.org/10.1016/j.biomaterials.2021.120776

65. Abedin-Do A, Zhang Z, Douville Y, et al. Electrical stimulation promotes the angiogenic potential of wound-healing fibroblasts. Front Bioeng Biotechnol. 2022;10:989888. https://doi.org/10.3389/fbioe.2022.989888

66. Arora M, Harvey LA, Glinsky JV, et al. Electrical stimulation for treating pressure ulcers. Cochrane Database Syst Rev. 2020;(1):CD012196. https://doi.org/10.1002/14651858.CD012196.pub2

67. Lu B, Yuk H, Lin S, et al. Pure PEDOT:PSS hydrogels. Nat Commun. 2019;10(1):1043. https://doi.org/10.1038/s41467-019-09003-5

68. Han B, Bischof JC. Direct cell injury associated with eutectic crystallization during freezing. J Biomech Eng. 2004;126(2):196–203. https://doi.org/10.1115/1.1688778

69. Liu J, Wang X, Li D, et al. Thermal conductivity and elastic constants of PEDOT:PSS with high electrical conductivity. Macromolecules. 2015;48(3):585–591. https://doi.org/10.1021/ma502099t

70. Lenz A, Kariis H, Pohl A, Persson P, Ojamäe L. The electronic structure and reflectivity of PEDOT:PSS from density functional theory. Chem Phys. 2011;384(1–2):44–51. https://doi.org/10.1016/j.chemphys.2011.05.003

71. Park H, Lee SH, Kim FS, et al. Enhanced electrical properties of PEDOT:PSS through a post-treatment process. J Mater Chem A. 2014;2(19):6532–6539. https://doi.org/10.1039/C3TA14960A

72. Inoue A, Yuk H, Lu B, Zhao X. Strong adhesion of wet conducting polymers on diverse substrates. Sci Adv. 2020;6(12):eaay5394. https://doi.org/10.1126/sciadv.aay5394

73. Suarez-Arnedo A, Torres Figueroa F, Clavijo C, et al. An image J plugin for the high throughput image analysis of in vitro scratch wound healing assays. PLoS One. 2020;15(8):e0232565. https://doi.org/10.1371/journal.pone.0232565

74. Piccinini F, Kiss A, Horvath P. CellTracker (not only) for dummies. Bioinformatics. 2016;32(6):955–957. https://doi.org/10.1093/bioinformatics/btv686

75. Srirussamee K, Mobini S, Cassidy NJ, Cartmell SH. Direct electrical stimulation enhances osteogenesis by inducing Bmp2 and Spp1 transcripts and PKCδ protein expression. J Tissue Eng Regen Med. 2019;13(8):1362–1372. https://doi.org/10.1002/term.2878

76. Rouabhia M, Park HJ, Zhang Z. Electrically stimulated keratinocytes produce or secrete anti-inflammatory cytokines and growth factors. J Wound Care. 2019;28(7):424–431. https://doi.org/10.12968/jowc.2019.28.7.424

77. Sebastian A, Iqbal SA, Colthurst J, Bayat A. Electrical stimulation enhances epidermal proliferation in human fetal skin constructs by activation of the β-catenin signaling pathway and altered expression of notch-1 and connexin 43. J Invest Dermatol. 2011;131(1):104–114. https://doi.org/10.1038/jid.2010.264

78. Weiss DS, Kirsner R, Eaglstein WH. Electrical stimulation and wound healing. Arch Dermatol. 1990;126(2):222–225. https://doi.org/10.1001/archderm.1990.01670260082012

79. Ashrafi M, Alonso-Rasgado T, Baguneid M, Bayat A. The efficacy of electrical stimulation in lower extremity cutaneous wound healing: a systematic review. Exp Dermatol. 2017;26(2):171–178. https://doi.org/10.1111/ exd.13179